Design of Artificial Neurons of Memristive Neuromorphic Networks Based on Biological Neural Dynamics and Structures

Xiaosong Li, Jingru Sun, *Member, IEEE*, Yichuang Sun, *Senior Member, IEEE*, Chunhua Wang, Qinghui Hong, Sichun Du, Jiliang Zhang, *Senior Member, IEEE*

***Abstract*—Memristive neuromorphic networks have great potential and advantage in both technology and computational protocols for artificial intelligence. Efficient hardware design of biological neuron models forms the core of research problems in neuromorphic networks. However, most of the existing research has been based on logic or integrated circuit principles, limited to replicating simple integrate-and-fire behaviors, while more complex firing characteristics have relied on the inherent properties of the devices themselves, without support from biological principles. This paper proposes a memristor-based neuron circuit system (MNCS) according to the microdynamics of neurons and complex neural cell structures. It leverages the nonlinearity and non-volatile characteristics of memristors to simulate the biological functions of various ion channels. It is designed based on the Hodgkin-Huxley (HH) model circuit, and the parameters are adjusted according to each neuronal firing mechanism. Both PSpice simulations and practical experiments have demonstrated that MNCS can replicate 24 types of repeating biological neuronal behaviors. Furthermore, the results from the Joint Inter-spike Interval(JISI) experiment indicate that as the background noise increases, MNCS exhibits pulse emission characteristics similar to those of biological neurons.**

***Index Terms*—Memristor, Neuromorphic networks, Hodgkin Huxley model, Ion chanel, Neurodynamics.**

I. Introduction

SINCE the emergence of large-scale models, like ChatGPT, people have once again experienced the power and practicality of artificial intelligence (AI) up close. However, the integration density of silicon-based hardware has reached its physical limits, combined with the high power consumption of von Neumann architecture, resulting in a bottleneck in the development of AI [1]. This is particularly evident in mobile robotics, where existing chips and portable power supplies cannot meet the operational requirements of large-scale artificial intelligence algorithms. Compared to existing artificial intelligence networks, the biological brain possesses a unique structure that integrates storage and computation, providing distinct advantages in terms of energy consumption, chaotic behavior, nonlinearity, and parallel processing capabilities [2]. This is illustrated in Fig.1a. Hence, the development of neuromorphic networks is a crucial pathway to advance AI towards artificial general intelligence (AGI) [3]–[6].

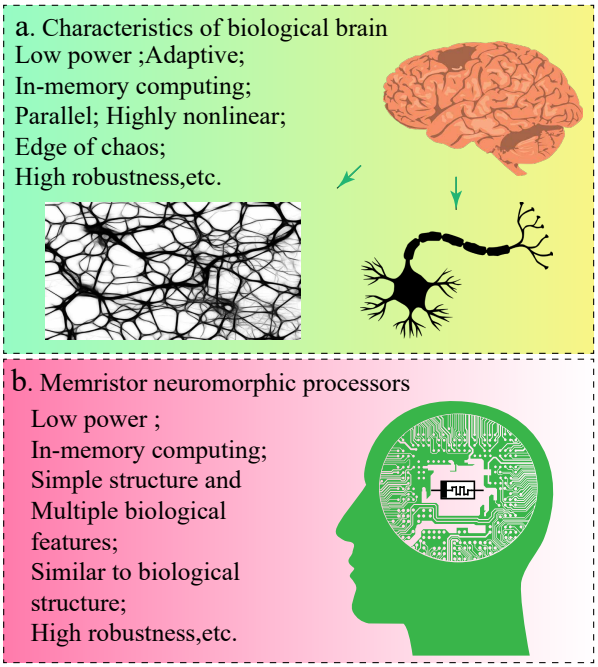

Fig. 1. Biological neurons vs. Memristor-based neural systems.

Neuron serves as the core computational unit in biological neural networks, over 20 distinct firing characteristics have been identified, to form intricate and dynamic computational systems. Neurons are connected through complex plasticity synapses and form an extraordinary biological intelligence with cognition, memory, and consciousness. Therefore, research on neuromorphic networks of artificial neurons primarily encompasses two main aspects: replicating neuronal connection pathways [7], [8] and fine neural circuit design [9], [10], as illustrated in Fig.1b. However, constrained by the computing power of simplified neuronal models, artificial neural networks still cannot show the same computing capabilities as the human brain due to insufficient activation or poor robustness et al [11]. In addition, highly biomimetic neural

Manuscript received X X, 2023.

Xiaosong Li, Jingru Sun are with the College of Computer Science and Electronic Engineering, Hunan University, Changsha 410082, China and Chongqing Research Institute, Hunan University, Chongqing 401120, China. E-mail:liguangbi, jt_sunjr@hnu.edu.cn.

Chunhua Wang, Qinghui Hong and Sichun Du are with the College of Computer Science and Electronic Engineering, Hunan University, Changsha 410082, China. E-mail:wch1227164, hongqinghui, jt_dsc@hnu.edu.cn.

Jiliang Zhang is with the College of Integrated Circuits, Hunan University, Changsha 410082, China. E-mail:zhangjiliang@hnu.edu.cn.

Yichuang Sun is with the School of Engineering and Computer Science, University of Hertfordshire, Hatfield AL10 9AB, UK. E-mail:y.sun@herts.ac.uk.

circuits based on complementary metal-oxide-semiconductor (CMOS) technology also bring problems such as reduced hardware integration density and increased power consumption [12], [13]. However, in order to achieve low latency and high nonlinearity in neural morphological computation, similar to the biological brain, the computational capabilities of neurons should not be overlooked. To simultaneously address low power consumption and high integration density, it is necessary to break through the computational architecture of traditional computers and leverage the inherent characteristics and coordinated operation of various organelles, just like neurons, to accomplish complex calculations.

Memristors provide a novel approach to the realization of neuromorphic networks [14], [15]. First, compared to silicon-based devices, memristors exhibit a smaller size, lower power consumption, and greater ease of integration [16], [17]. Second, their nonlinear and non-volatile characteristics closely resemble those of biological synapses [18]. Finally, the characteristics of single-compartment memristors closely resemble the ion channel permeability, which is the core of the firing behavior of neurons, intricately linked to the activity of Na^+, K^+, and Ca^{2+}. As shown in Fig. 1, the characteristic of memristor-based neuron circuit system (MNCS) exhibits striking similarities to neurons [19]. Therefore, memristor has been wildly used in the design of neurons [20], synapses [21], [22], and chaotic circuits [23], [24], to enhance integration densities, and reduce energy consumption [25], [26].

Currently, research on memristor-based artificial neurons focuses on two aspects. One aspect is through the inherent properties of memristors that simulate a wide range of neuronal characteristics. These memristor neuron circuits have a simple structure, complex computation, and the ability to exhibit multiple neuronal properties [27]–[29]. However, compared to biological neurons, they exhibit lower robustness, and limited biological interpretability due to the absence of neuronal structures. The other aspect employs memristors to simulate the diverse organelles of neurons and construct highly nonlinear memristor neuron circuits [19], [30]. These circuits have been demonstrated to exhibit various neuronal characteristics, including all-or-nothing spiking, refractory period.

Nevertheless, most of these firing behaviors in memristor-based neuron circuits are explained by the Leaky Integrate-and-Fire (LIF) model [31], [32]. In comparison to the HH model [33], [34], the LIF model has a simplified biomimetic structure, resulting in fewer neural computational characteristics. Conversely, the Hodgkin-Huxley (HH) model is designed based on the structural and computational characteristics of neurons. By adjusting its parameters, the HH can accurately reproduce the majority of known neuronal firing behaviors [35], [36]. However, few works strictly rely on the HH model for neuronal circuit design due to its excessive complexity. As a consequence, even though the neuronal structure is considered [19], [30], most memristor-based neuron circuits still rely on the inherent characteristics of the memristor to achieve specific neuronal firing behaviors, such as inhibition-induced bursting [37], [38]. Neurons possess strong robustness. When one organelle ceases to function, substitute organelles with similar functions, such as astrocytes, will take over the entire signal transmission process. However, current work neglects the close collaboration between organelles and relies solely on high-order nonlinear devices to simulate neuron characteristics, which results in poor robustness and low reliability of the artificial neural network and deviates from the original goal of bionics, and cannot be trained, learned, and stored like a biological neural network.

To emulate the dynamics and structure of neuron and enhance the robustness and biological interpretability of memristor-based neurons, this paper proposes a memristor model to adapt various ion channel dynamics. Furthermore, based on the HH model circuit and dynamic equation, a highly biomimetic MNCS is proposed. To enhance biological interpretability, the electronic devices in the MNCS are directly mapped to organelles of neurons. To validate the reliability of the MNCS, we conducted simulation experiments using PSpice and performed circuit experiments using a memristor circuit simulator built with COMS components. The results of both tests demonstrated that the MNCS is capable of reproducing 24 different types of neuron characteristics, including mixed mode, inhibition-induced spiking, inhibition-induced bursting, resonator, and various other complex firing behavior. Additionally, to verify the biomimetic characteristics of the MNCS, the Joint Inter-spike Interval (JISI) experiments are conducted, and the results are compared with those of biological experiments, which further confirms the biological plausibility of the MNCS.

The rest of this paper is organized as follows. Section II describes the physiological process of neuron firing, the memristive model of ion channels, and the neuronal dynamics equation. Section III presents the circuit design of MNCS, computer simulation experimental results, circuit experimental results, and JISI experimental results. Section IV provides a comparative analysis of MNCS with previous research. Section V presents the conclusions.

II. Neuronal Firing Mechanism and Ion Channel Memristor Model

In the intricate network of the biological nervous systems, a multitude of neuron types can be found, each with a unique firing mechanism. Even within a single type of neuron, multiple firing mechanisms can be observed [39]. In this section, we explore the typical neuronal firing mechanisms primarily from a biological standpoint, delve into the ion channels' dynamics, and introduce the memristor model, offering an alternative to the biological ion channel functionality.

Some specialized terminology needs to be explained in advance. Resting membrane potential refers to the voltage difference, with the outside of the cell membrane being positively charged and the inside being negatively charged, that exists across the cell membrane when it is not stimulated. Polarization refers to the process of making the cell membrane potential more negative, approaching the resting membrane potential. Depolarization refers to the process of making the cell membrane potential more positive, moving away from the negative resting membrane potential. Hyperpolarization refers to the process of making the cell membrane potential more

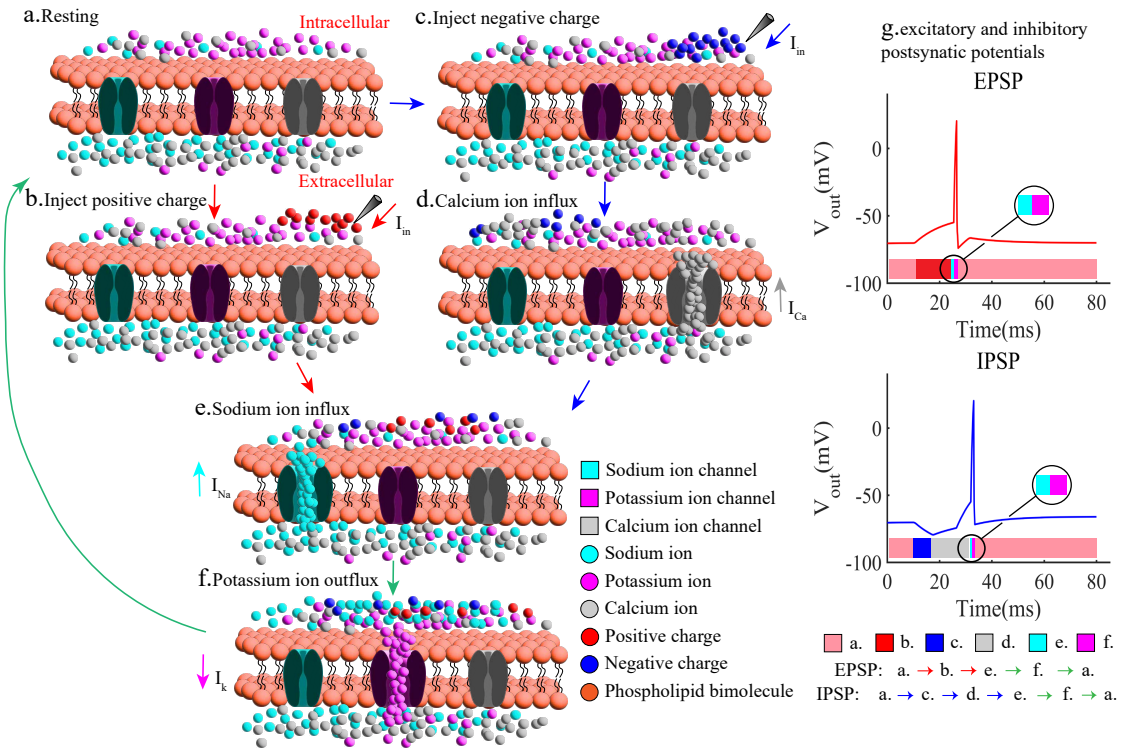

Fig. 2. Microscopic mechanism of neuronal cell firing. a) Resting state; b) Injecting positive charges into the neuronal cell; c) Sodium ions flow into the cell from the extracellular space; d) Potassium ions flow out of the cell from the intracellular space to the extracellular environment.; e) Injecting negative charges into the neuronal cell; f) Calcium ion flow into the cell from the extracellular space; g) Excitatory and inhibitory postsynaptic potentials(EPSP and IPSP).

negative, moving away from the normal resting membrane potential.

A. Typical neuronal firing mechanisms

The fundamental reason for generating different firing characteristics lies in the activation and deactivation of distinct ion channels under various stimuli [40]. The ion channels primarily involved in generating action potentials are Na^+, K^+, and Ca^{2+} channels. When a neuron is not generating an action potential, major ion channel groups are in an inactive state, known as the resting state, as depicted in Fig. 2a. The Nernst potentials for Na^+ and Ca^{2+} are $55mV$ and $118mV$, respectively, due to their higher concentrations outside the neuronal cell. In contrast, the concentration of K^+ inside the cell is higher than outside, so the Nernst potential for K^+ is $-77mV$. When the neuron is at rest, non-voltage-gated K^+ channels are activated, allowing K^+ to move freely across the cell membrane. Due to the movement of K^+ and the influence of charged particles, the membrane potential stays around $-71mV$ in the resting state [39].

Depending on the polarity of the input current, neurons can produce either Excitatory Postsynaptic Potentials (EPSP) or Inhibitory Postsynaptic Potentials (IPSP). EPSP occurs when positive charges are injected into the neuron, causing the membrane potential to increase gradually and leading to the depolarization of the neuronal cell, as shown in Fig.2b. Once the membrane potential reaches a certain threshold of around $-55mV$, there is a rapid activation of the Na^+ channels, which allows for a significant influx of Na^+ into the cell. This leads to further depolarization of the neuron, as shown in Fig. 2e. When the membrane potential reaches the activation threshold of the K^+ channels (typically around $20mV$), the K^+ channel groups rapidly activate, resulting in a significant efflux of K^+ from the cell, as shown in Fig. 2f. This leads to a swift decrease in membrane potential, causing hyperpolarization of neurons. During this process, the Na^+ channels also undergo inactivation. When the membrane potential decreases to the inactivation threshold of the K^+ channels (typically around $-76mV$), the K^+ channels undergo a slow process of inactivation, leading to the neuron to return to the resting state, thereby completing an action potential. Fig. 2g shows the T-V curve of EPSP.

Compared to EPSP, the ion channels and stimulation methods involved in IPSP are different [41]. When the neuron cell is in a resting state, negative charges are injected into the cell, as depicted in Fig. 2c. During this period, the membrane potential decreases, leading to neuron hyperpolarization. When the activation threshold of the T-type Ca^{2+} channel is reached (typically around $-80mV$) [42], the T-type Ca^{2+} channel activates. Due to the concentration gradient, a significant influx of Ca^{2+} occurs, leading to depolarization of the nerve cell, ultimately reaching the activation threshold of the Na^+ channel, as illustrated in Fig. 2d. Subsequently, the firing process of EPSP is iterated, leading to the completion of the action potential. The T-V curve of IPSP is shown in Fig. 2g. Due to the fast activation and slow deactivation of T-

type Ca^{2+} channels, neurons will continue to generate action potentials until the T-type Ca^{2+} channels are fully inactivated [43], [44].

Bursting is a distinctive pattern of neuronal firing closely linked to Ca^{2+}-gated K^+ channels [41]. In neuronal experiments, the use of apamin, a specific blocker of small conductance (SK) Ca^{2+}-gated K^+ channels, can induce bursting activity in neurons [45]. One possible explanation is that during the generation of the action potential, apamin blocks a portion of the K^+ channels, preventing the efflux of K^+ from the cells promptly. This results in the inability of membrane potential to reach the inactivation threshold of Na^+ channels, thereby delaying the inactivation of Na^+ channels. Consequently, a continuous influx of Na^+ into the cell results in the repetitive activation and deactivation of functional K^+ channels within a short period, thereby giving rise to bursting activity [39], [41].

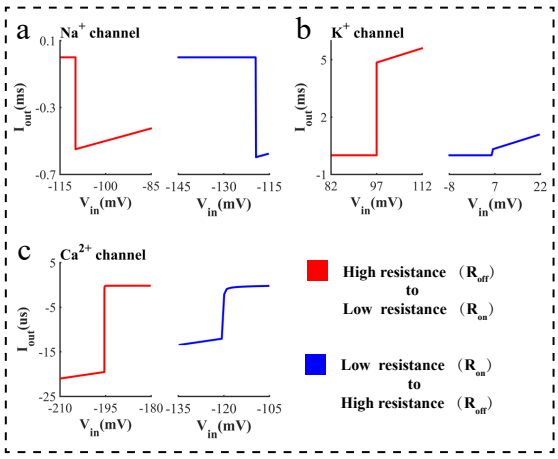

Fig. 3. The $V-I$ characteristic curves of sodium, potassium, and calcium ion channel memristors.

B. Ion channel memristor

From the above analysis, it can be known that ion channel organelles play an essential role in neurons' firing behavior. The intricate biological attributes of ion channels can be faithfully replicated through the utilization of single-compartment memristors. In particular, memristors engineered with materials like niobium oxide and vanadium oxide excel in this regard [19], [30], [46]. In this paper, according to the biological characteristics of each ion channel, a memristor circuit model was designed and simulated with PSpice [47]. Furthermore, a memristor circuit was designed, and circuit experiments were carried out, to verify the accuracy and biological rationality of the ion channel memristor model.

Na^+ channel memristor: Among various ion channels, the Na^+ channel belongs to the fast-activating and fast-inactivating types. Its function is to facilitate the rapid depolarization of neurons. Based on the activation and deactivation thresholds observed in Na^+ channels within neurons, it is identified that there are two thresholds for the Na^+ channel memristor model. The dynamic equation of the memristor is expressed by Eq. (1), (2), and (3). Table I provides all parameters involved in the dynamic equations of the memristor model. Fig. 3a, 3b, and 3c illustrate the $V-I$ curves of Na^+, K^+, Ca^{2+} channel memristors, respectively. In Fig. 3, the blue curve represents the process of the memristor switching from a low-resistance state to a high-resistance state, while the red curve represents the opposite.

$$V(t) = R_{off} - x \cdot \Delta R \cdot i(t) \tag{1}$$

$V(t)$ represents the voltage passing through the memristor at t moment, t denotes time, and R_{off} corresponds to the maximum resistance of the memristor. The x represents the resistance coefficient of change, which fluctuates with the current and time based on the resistance coefficient change Eq. (2) or (4). The $i(t)$ represents the current passing through the memristor at t moment, and ΔR refers to the difference between the maximum resistance R_{off} and the minimum resistance R_{on} of the memristor. The values of R_{off} and R_{on} are determined by the rate at which ions flow through the ion channels.

$$\frac{\mathrm{d}x}{\mathrm{d}t} = \begin{cases} q_1 \cdot k_{on}^{b_1} \cdot f_1(x) \cdot i(t) \cdot \Delta R, & V(t) < V_{th1} \\ 0 \quad , & V_{th2} > V(t) \geq V_{th1} \\ q_2 \cdot k_{off}^{b_2} \cdot f_2(x) \cdot i(t) \cdot \Delta R, & V(t) \geq V_{th2} \end{cases} \tag{2}$$

where $f(x)$ represents a window function that is utilized to modify the nonlinear variation characteristics of the memristor model. It is expressed by Eq. (3). The coefficients q_1, q_2, k_{on}, k_{off}, b_1, b_2 are used to adjust the rate of resistance change of the memristor.

$$f(x) = \begin{cases} a_1 \cdot (1+x)^{p_1} \\ a_2 \cdot (1+x)^{p_2} \end{cases} \tag{3}$$

In Eq. (3), a_1, a_2, p_1, p_2 represent the coefficients used to adjust the nonlinear variation characteristics of the memristor. In order to replicate activation characteristics of Na^+ channels, the resistance switching speed of the memristor model is intentionally set to be remarkably fast. This results in a $V-I$ curve that is nearly perpendicular to the x-axis, as shown in Fig. 3a.

K^+ channel memristor: K^+ channels demonstrate rapid activation and gradual inactivation properties. In fact, the activation speed of K^+ channels is even faster than that of Na^+ channels. Two thresholds for the memristor add are before based on the characteristics of the K^+ channel. By fine-tuning the parameters of Eq. (4), the resistance switching speed of the memristor can be adjusted to align with the properties exhibited by potassium ion channels. The dynamic behavior of the memristor is described by Eq. (1), (3), and (4) in the dynamic equation.

$$\frac{\mathrm{d}x}{\mathrm{d}t} = \begin{cases} q_1 \cdot k_{on}^{b_1} \cdot f_1(x) \cdot i(t) \cdot \Delta R, & V(t) > V_{th1} \\ 0 \quad , & V_{th1} \geq V(t) > V_{th2} \\ k_{off}^{b_2} \cdot f_2(x) \cdot i(t)^{q_2} \cdot \Delta R, & V(t) \leq V_{th2} \end{cases} \tag{4}$$

TABLE I
PARAMETERS OF SODIUM, POTASSIUM, AND CALCIUM ION CHANNEL MEMRISTORS.

ID	Ion CH	R_{off}	R_{on}	V_{th1}	V_{th2}	b_1	b_2	p_1	p_2	k_{off}	q_1	q_2	Dynamical Eq.
1	**Na^+ CH**	$1M\Omega$	200Ω	$-110mV$	$-119.5mV$	15	2	4	2	2	-	-	(1), (2), (3)
2	**K^+ CH**	$1M\Omega$	20Ω	$97mV$	$7mV$	18	-9.8	4	2	2	1.05	-0.51	(1), (3), (4)
3	**K^+ CH2**	$11M\Omega$	20Ω	$97mV$	$40mV$	18	-9.8	4	2	2	1.05	-0.51	(1), (3), (4)
4	**Ca^{2+} CH**	$1M\Omega$	$10k\Omega$	$-195mV$	$-120mV$	7	5	1.2	2.1	2	1	1	(1), (2), (3)
5	**K^+ CH3**	$1M\Omega$	20Ω	$97mV$	$40mV$	18	-9.8	4	2	2	1.05	-0.51	(1), (3), (4)
6	**K^+ CH4**	$1M\Omega$	20Ω	$97mV$	$7mV$	18	-9.8	4	2	0.01	1.05	-0.51	(1), (3), (4)
7	**Ca^{2+} CH2**	$20k\Omega$	$10k\Omega$	$-195mV$	$-120mV$	7	5	1.2	2.1	2	1	1	(1), (2), (3)
8	**K^+ CH5**	$1M\Omega$	$1k\Omega$	$15mV$	$7mV$	7	7	4	2	2	1	1	(1), (2), (3)
9	**Ca^{2+} CH3**	$1M\Omega$	$30k\Omega$	$-184mV$	$-192mV$	12	12	4	2	2	1	1	(1), (2), (3)
10	**K^+ CH6**	$1M\Omega$	500Ω	$97mV$	$40mV$	18	1	4	2	0.01	1.05	1	(1), (3), (4)

Note 1 : In all memristors, the values of a_1 and a_2 are 1, and the value of k_{on} is 2.
Note 2 : The symbol '-' represents an empty value.
Note 3 : K^+ CH2: K^+ channel for bursting; K^+ CH3: Ca^{2+}-gated K^+ channel; K^+ CH4: Special K^+ channel; K^+ CH5: Non-voltage-gated K^+ channel; Ca^{2+} CH: T-type Ca^{2+} channel; Ca^{2+} CH2: Dysfunctional Ca^{2+} channel; Ca^{2+} CH3: L-type Ca^{2+} channel;

From the $V-I$ curve depicted in Fig. 3b for the K^+ channel memristor, it is clear that the memristor undergoes a rapid transition in resistance from R_{off} to R_{on}, like Na^+ channel. The transition from R_{on} to R_{off} occurs relatively slowly, and the $V-I$ curve exhibits a gradual slope. This characteristic aligns with the biological properties of K^+ channels. It is important to note that the resistance recovery speed of K^+ channel memristors needs to be regulated within an appropriate range. If it is too fast, the neuron circuit may not hyperpolarize sufficiently, whereas if it is too slow, it can impact the frequency of pulse firing.

Ca^{2+} channel memristor: In neurons, there exist various types of Ca^{2+} channels. However, the specific Ca^{2+} channels implicated in IPSP are predominantly the T-type Ca^{2+} channels [42]. Hence, it is primarily focused on designing the memristor model based on the specific attributes of the T-type Ca^{2+} channel. As mentioned earlier, the T-type Ca^{2+} channel is characterized as a fast-activating and slow-inactivating type of ion channel. During the polarization of neurons, the T-type Ca^{2+} channel is activated and gradually inactivated throughout the depolarization process. In a similar manner, two trigger thresholds for the memristor are established based on the specific characteristics of the T-type Ca^{2+} channel. Furthermore, by taking into account the activation properties of the T-type Ca^{2+} channel, the resistance switching speed of the memristor is fine-tuned using Eq. 2. The dynamic behavior of the memristor is described by Eq. 1, 2, and 3.

Similar to K^+ channels, Ca^{2+} channels also demonstrate fast activation and slow inactivation characteristics. As a result, the $I-V$ curves of Ca^{2+} channel memristors closely resemble those of K^+ channel memristors, as shown in Fig. 3c. It is worth noting that an excessive influx of Ca^{2+} into neurons can lead to abnormal neuronal firing, resulting in conditions such as epilepsy or QT syndrome [48], [49]. Therefore, the rate of Ca^{2+} flow through ion channels is not as high as that of Na^+ or K^+. To emulate this neuronal characteristic, the resistance value R of the Ca^{2+} channel memristor is deliberately set to a relatively high level in order to prevent abnormal firings in MNCS.

C. Dynamics of MNCS

Due to its classification as a fine neuronal-biomimetic circuit, MNCS can be comprehensively explained by utilizing the dynamic equations of the HH model. The conservation of electric charge on a piece of membrane implies that the applied current $I(t)$ may be split into two parts, a capacitive current $I_C(t)$ charges the capacitor C, and components I_k pass through the ion channels.

$$I(t) = I_c(t) + \sum_k I_k, \tag{5}$$

where the sum runs over all ion channels. From the definition of capacitance $C = q/u$, q is the charge and u is the voltage across the capacitor, we have the charging current $I_C(t) = C \cdot du/dt$. Hence from Eq. (5)

$$C \cdot \frac{du}{dt} = -\sum_k I_k + I(t). \tag{6}$$

With the incorporation of Ca^{2+} channels, an extra dimension must be included in the dynamic equations of the HH model to adequately describe MNCS. The dynamic equations of MNCS can be represented by

$$\begin{aligned}\sum_k I_k = g_{Na} \cdot (u - E_{Na}) + g_k \cdot (u - E_k) + \\ g_{Ca} \cdot (u - E_{Ca}) + g_L \cdot (u - E_L).\end{aligned} \tag{7}$$

The parameters g_{Na}, g_K, and g_{Ca} denote the alterations in the conductance of Na^+, K^+, and Ca^{2+} throughout the process of action potential generation. The values of these variables are determined collectively by Eq.(1), (2), (3), and (4). The changes in conductance of the leakage channel are represented by g_L. The parameters E_{Na}, E_K, E_{Ca}, and E_L are the reversal potentials, u represents the membrane potential.

III. SIMULATION AND PRACTICAL EXPERIMENTS

In the previous section, the firing mechanism of biological neurons has been described. In this section, we replace the organelles in neurons with electronic devices and construct neural circuit systems based on the structure of neurons to

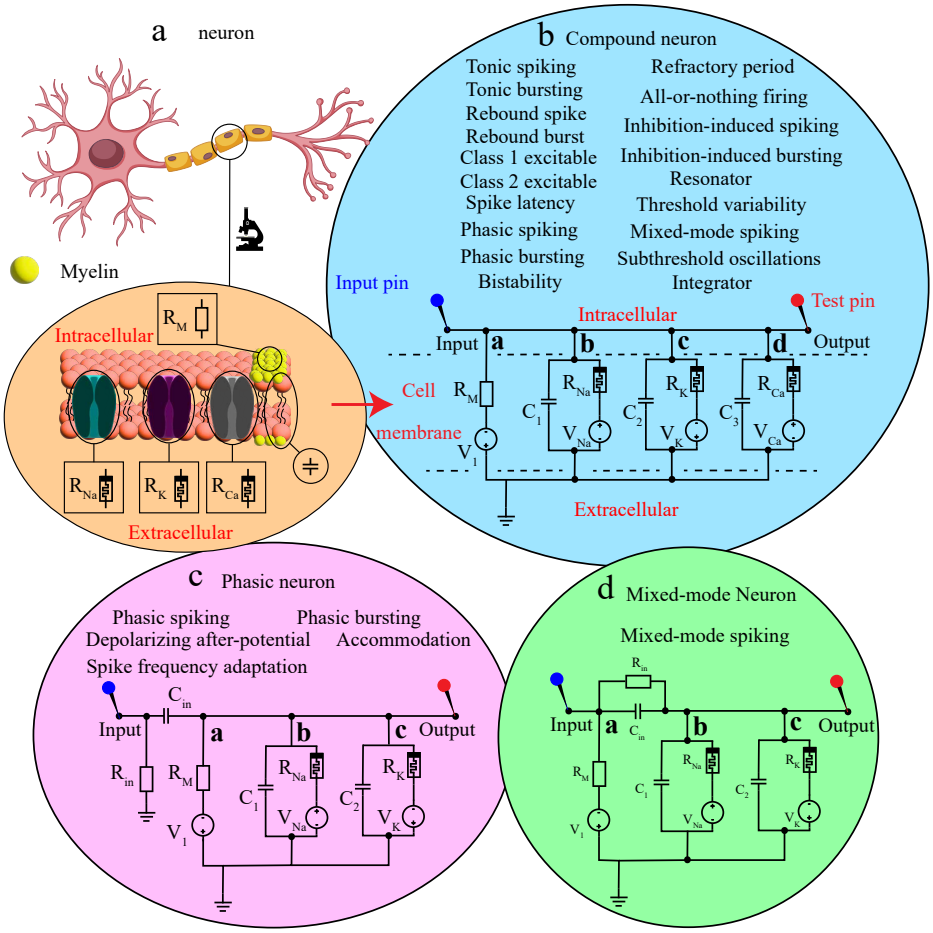

Fig. 4. Memristor-based Neuron Circuit System. a) Electronic Devices Corresponding to Neuronal Organelles; b) Compound Neuron(CN), Highly consistent with neuronal structures, the compound neuron is capable of faithfully replicating the vast majority of neuronal discharge characteristics; c) Phasic Neuron(PN), The PN lacks biological knowledge support in certain mechanisms, but it is capable of reproducing specific neuronal discharge characteristics; d)Mixd-mode Neuron(MN), The Mixed-mode Neuron exclusively replicates a single type of neuronal discharge characteristic, providing a basis for comparison with the CN.

replicate the majority of neuronal characteristics. Simulation and experiments are carried out to verify the effectiveness of the proposed circuit systems.

A. Memristive-based Neuronal Circuit System

As described in Section II, the outflow of K^+ inside neuronal cells generates a resting potential of approximately $-71mV$. Therefore, in the MNCS, a fixed resistor R_k^* is used to simulate the non-voltage-gated K^+ channel, and it is connected in series with a $-77mV$ DC power supply to mimic the outflow of K^+. As shown in the branch a in Fig. 4b, 4c, 4d.

The MNCS can be divided into two sub-circuit systems, Compound Neuron (CN) and Phasic Neuron (PN). As a comparative circuit, the Mixed-mode Neuron (MN) does not belong to the MNCS. For CN, it is designed entirely based on the structure of neurons. As shown in Fig. 4b, the area above dashed line 1 represents the intracellular region, while the area below dashed line 2 represents the extracellular region. The region between dashed lines 1 and 2 represents the cell membrane and the organelles present on the membrane. As shown in Fig 4a, ion channels, and other organelles are embedded in the cell membrane. According to the principles of circuitry, the organelles on the membrane and the cell membrane itself are effectively connected in parallel. Therefore, in the HH model circuit, the individual resistors representing ion channels and the capacitor representing the cell membrane are connected in parallel. The CN, PN, and MN, following the design of the Hodgkin-Huxley model circuit, also inherit this structure. In CN, PN, and MN, the R_{na}, R_k, and R_{ca} represent ion channel memristors, which serve as substitutes for the variable resistors in the HH model circuit, whereas V_2, V_3, and V_4 represent the Nernst potentials resulting from the concentration gradients of various ions between the interior and exterior of the neuronal cell.

The capacitors C_1, C_2, and C_3 correspond to the cell membranes surrounding the respective ion channels in their local regions. It is important to note that when action potentials propagate along axons, the Na^+, K^+, and Ca^{2+} channels that undergo rapid activation are confined to a small region. The capacitance of the biological capacitor formed by the lipid bilayer remains unchanged, which means that C_1, C_2,

TABLE II
THE PARAMETERS OF MEMRISTOR-BASED NEURON CIRCUIT SYSTEM COMPUTER SIMULATION TEST.

Category	$\mathbf{R_{in}}$	$\mathbf{C_{in}}$	$\mathbf{C_1}$	$\mathbf{C_2}$	$\mathbf{C_3}$	$\mathbf{N_m^b}$	$\mathbf{V_2^b}$	$\mathbf{N_m^c}$	$\mathbf{V_3^c}$	$\mathbf{N_m^d}$	$\mathbf{V_4^d}$	Circuit
Phasic spiking	$6k\Omega$	$1.5\mu F$	$1.5\mu F$	$1.5\mu F$	$1.5\mu F$	1	$55mV$	2	$-77mV$	-	-	PN
	-	-	$1.5\mu F$	$1.5\mu F$	$1.5\mu F$	1	$55mV$	6	$-77mV$	-	-	CN
Phasic bursting	$6k\Omega$	$1.5\mu F$	$0.5\mu F$	$0.5\mu F$	$0.5\mu F$	1	$55mV$	5	$-77mV$	-	-	PN
	-	-	$2\mu F$	$2\mu F$	$2\mu F$	1	$55mV$	5	$-77mV$	6	-77mV	CN
Spike frequency adaptation	$6k\Omega$	$30\mu F$	$2\mu F$	$2\mu F$	$2\mu F$	1	$55mV$	2	$-77mV$	-	-	PN
Depolarizing after-potential	$10k\Omega$	$1.5\mu F$	$1.5\mu F$	$1.5\mu F$	$1.5\mu F$	1	$55mV$	2	$-77mV$	-	-	PN
Accommodation	$10k\Omega$	$1\mu F$	$1\mu F$	$1\mu F$	$1\mu F$	1	$55mV$	2	$-77mV$	-	-	PN
Tonic spiking	-	-	$2\mu F$	$2\mu F$	$2\mu F$	1	$55mV$	2	$-77mV$	-	-	CN
Tonic bursting	-	-	$2\mu F$	$2\mu F$	$2\mu F$	1	$55mV$	2	$-77mV$	-	-	CN
Rebound spike	-	-	$2\mu F$	$2\mu F$	$2\mu F$	1	$55mV$	2	$-77mV$	3	$118mV$	CN
Rebound bursting	-	-	$2\mu F$	$2\mu F$	$2\mu F$	1	$55mV$	5	$-77mV$	3	$118mV$	CN
Class 1 excitable	-	-	$2\mu F$	$2\mu F$	$2\mu F$	1	$55mV$	2	$-77mV$	-	-	CN
Class 2 excitable	-	-	$0.3\mu F$	$0.3\mu F$	$0.3\mu F$	1	$55mV$	2	$-77mV$	-	-	CN
Spike latency	-	-	$1.5\mu F$	$1.5\mu F$	$1.5\mu F$	1	$55mV$	2	$-77mV$	9	$118mV$	CN
Refractory period	-	-	$1.5\mu F$	$1.5\mu F$	$1.5\mu F$	1	$55mV$	2	$-77mV$	-	-	CN
All-or-nothing firing	-	-	$1.5\mu F$	$1.5\mu F$	$1.5\mu F$	1	$55mV$	2	$-77mV$	-	-	CN
Inhibition-induced spiking	-	-	$1.5\mu F$	$1.5\mu F$	$1.5\mu F$	1	$55mV$	2	$-77mV$	3	$118mV$	CN
Inhibition-induced bursting	-	-	$1.5\mu F$	$1.5\mu F$	$1.5\mu F$	1	$55mV$	2	$-77mV$	5	$118mV$	CN
Resonator	-	-	$1.5\mu F$	$1.5\mu F$	$1.5\mu F$	1	$55mV$	2	$-77mV$	-	-	CN
Integrator	-	-	$1.5\mu F$	$1.5\mu F$	$1.5\mu F$	1	$55mV$	2	$-77mV$	-	-	CN
Threshold variability	-	-	$1.5\mu F$	$1.5\mu F$	$1.5\mu F$	1	$55mV$	2	$-77mV$	3	$118mV$	CN
Subthreshold oscillations	-	-	$1.5\mu F$	$1.5\mu F$	$1.5\mu F$	1	$55mV$	2	$-77mV$	3	$118mV$	CN
Dysfunctional Ca channel	-	-	$1.5\mu F$	$1.5\mu F$	$1.5\mu F$	1	$55mV$	2	$-77mV$	7	$118mV$	CN
Mixed mode	$45k\Omega$	$1\mu F$	$1\mu F$	$1\mu F$	$1\mu F$	1	$55mV$	2	$-77mV$	-	-	PN
	-	-	$1.5\mu F$	$1.5\mu F$	$1.5\mu F$	1	$55mV$	2	$-77mV$	5	$-77mV$	CN
Bistability	-	-	$1.5\mu F$	$1.5\mu F$	$1.5\mu F$	1	$55mV$	2	$-77mV$	8	$-77mV$	CN
Excitation block	-	-	$1.5\mu F$	$1.5\mu F$	$1.5\mu F$	1	$55mV$	2	$-77mV$	10	$-77mV$	CN

Note 1: The symbol '-' represents an empty value.
Note 2: $\mathbf{N_m^x}$ represents the unique identifier assigned to branch x within the MNCS. The specific memristor used in this branch is chosen based on the corresponding identifier found in Table I. The selected memristor is then configured according to the corresponding parameter settings associated with that identifier.
Note 3 : In addition to bistability, V_1 is $-71mV$. For bistability,V_1 is $-50mV$. All R_m are $2.7k\Omega$.

and C_3 have been set to equal values. In the PN and MN, there is no direct correspondence of C_{in} and R_{in} to specific organelles. The combination of C_{in} and R_{in} in the circuit is designed to temporarily disrupt the dynamic equilibrium of the neuronal circuit using the capacitor charging process, leading to the transient generation of action potentials or the generation of more action potentials. This design is only necessary for discharge modes such as Depolarizing after-potential, Accommodation, and Spike frequency adaptation. The generation of these action potentials relies on the inherent properties of C_{in} and R_{in} themselves, without reference to the structure and discharge mechanisms of biological cells, resulting in relatively low biological interpretability. PN leverages the inherent characteristics of the devices to achieve certain neuronal properties that are temporarily unattainable in CN. On the other hand, MN is used as a circuit of comparison with CN. Moreover, based on the parameter settings provided in Table I and II, CN, PN, and MN in schematic diagram Fig. 4 can successfully replicate 24 common discharge characteristics observed in neurons. The explanations for special parameter symbols used in the table are provided in the table notes. All of our simulation experiments were conducted using the PSpice simulation software. The simulation results for the 24 discharge characteristics are shown in Fig. 5. Each small colored block in the upper-left corner of each graph corresponds to the background color of the circuit depicted in Fig. 4, indicating that the result is generated by that circuit.

The five neuron firing behaviors depicted in Fig. 5a to 5e can be achieved through PN, while phasic spiking and phasic bursting can also be achieved through the CN. **Phasic spiking:** For the PN, the voltage change during the charging of capacitor C_{in} disrupts the balance of the MNCS, leading to an action potential. Once the voltage at both ends of the capacitor reaches a steady state, the MNCS returns to a resting state and no longer responds. The implementation mode of CN is significantly different. In CN, No.6 memristor in Table I is used to replace the K^+ channel memristor. Consequently, after an action potential is completed, the K^+ $CH4$ memristor fails to reset promptly, resulting in a sustained output that remains unchanged for a significant duration. **Phasic bursting:** In biological neurons, bursting is associated with the blocking of certain K^+ channels. Therefore, it is necessary to utilize the No.3 memristor from Table I circuit to simulate the blockage of the Ca^{2+}-gated K^+ channel. In the CN, besides utilizing the No. 3 memristor, it is also necessary to incorporate the No. 6 memristor from Table I to achieve single cluster firing.

Spike frequency adaptation: The basic principle of this firing characteristic is consistent with phasic spike. The variation in firing frequency is achieved through the nonlinear charging characteristics of the capacitor. By adjusting the input capacitance C_{in} and input resistance R_{in}, it is possible to modify the firing frequency and duration. **Depolarizing after-potential(DAP):** The implementation of DAP behavior in PN is achieved through the charging of capacitor C_{in} during action potential, which leads to a temporary increase in the voltage at both ends of C_{in}, exceeding the steady-state value and reaching V_{mxa}. Subsequently, when C_{in} discharges from V_{mxa} back to the steady-state value, the DAP phenomenon occurs. **Accommodation:** PN achieves this characteristic by leveraging the discrepancies in the charging and discharging speeds of capacitors C_{in}.

All of the firing characteristics that will be introduced next can be effectively implemented using the CN circuit. Regarding **Tonic spiking** and **Tonic bursting**, their implemen-

tation mechanism is fully consistent with the basic principles of neuronal firing, as described in detail in the previous sections. These behaviors can be achieved by setting the circuit parameters according to the values listed in Table I and II. **Rebound spiking and Rebound bursting:** The reason behind this characteristic is that the inhibitory small pulses cause the Ca^{2+} channels to be partially activated, allowing a small influx of Ca^{2+} into the neuron. As a result, the membrane potential rises, leading to the generation of action potentials. **Class 1 excitable and Class 2 excitable:** The main feature of these two characteristics is that different types of neurons generate action potentials at varying frequencies. In CN, different firing frequencies can be achieved by simultaneously adjusting the values of capacitors C_1, C_2, and C_3. The smaller the capacitance value, the higher the firing frequency. In neural cells, apart from the difference in cell membrane capacitance, the excessive activation or insufficient activation of cation channels, such as Na^+ channels, can also lead to action potential at different frequencies.

Spike latency: For spike latency, one possible explanation is that the L-type Ca^{2+} channel to be activated and slowly inactivated. When neurons receive a small stimulus, the L-type Ca^{2+} channel is activated [50], allowing a small amount of Ca^{2+} to flow into the cells continuously. The cells gradually depolarize, and an action potential is generated when the firing threshold is reached. The interval between the activation of the L-type Ca^{2+} channel and the emission of an action potential may range from several milliseconds to tens of milliseconds. **Refractory period:** The reason for this phenomenon is that during the action potential generation process, the ion channel is already activated and the typical inputs during this process do not significantly affect the state of the ion channel. As a result, the neuron does not respond to these inputs. In MNCS, the ion channel memristor is in the R_{on} state, and the resistance value is minimally affected by the input current. As a result, MNCS does not exhibit a significant response to the input current. **All-or-nothing firing:** This is a fundamental characteristic of all neuron cells. The firing mechanism aligns with the process of action potential generation, which has been extensively discussed in the previous chapter.

Inhibition-induced spiking and Inhibition-induced bursting: Sustained inhibitory input currents maintain activation state of the Ca^{2+} channels, resulting in a persistent influx of Ca^{2+} into the neuron and causing repeated generation of action potentials. **Resonator:** This characteristic may be associated with certain specific negative ion channels, which is a reasonable speculation. High-frequency input may activate some negative ion channels, causing the two consecutive excitatory small pulses to fail in depolarizing the neuron to the threshold for generating action potentials. However, as long as the interval between the two excitatory small pulses is sufficiently long, this specific negative ion channel will remain inactive. The neuron will sustain a certain level of depolarization following the first excitatory small pulse, facilitating the second pulse to easily depolarize the neuron to the threshold for triggering an action potential. In the experiment, the delay switch replaced the function of this specific negative ion channel, thus confirming our hypothesis. **Integrator:** The situation with Integrator is the opposite of that with Resonator. An excitatory small pulse is unable to trigger neuronal firing, but when two excitatory small pulses within a short time are applied, the neuron can depolarize to the threshold for action potential generation. The longer the interval between the two excitatory small pulses, the more time the neuronal potential has to repolarize back to its initial level. This prevents the generation of action potentials.

Threshold variability: The situation of threshold variability is more complex. As shown in Fig.5s, an excitatory small pulse is unable to generate an action potential, but when an inhibitory small pulse is input to the neuron followed by the same excitatory small pulse, an action potential is generated. This is because the inhibitory small pulse can partially activate the T-type Ca^{2+} channel, placing the Ca^{2+} channel in a semi-activated state. As a result, a small amount of Ca^{2+} ions flows into the neuron, causing the neuron to reach a certain level of depolarization. This leads to an increase in membrane potential. Subsequently, when the same excitatory small pulse is applied, the neuron can depolarize further to reach the firing threshold, resulting in the generation of an action potential. On the surface, the inhibitory small pulse appears to modify the firing threshold for neuronal firing. However, the firing threshold of the neuron remains unchanged. The inhibitory small pulse simply increases the membrane potential of the neuron, thereby facilitating the firing of action potentials.

Subthreshold Oscillations: It has been proposed that when action potentials are generated, specific ions within the nerve cell are activated or partially activated. This causes both positive and negative ions to enter, disrupting the ion balance in the neuron. As a result, the neuron exhibits oscillatory behavior after the generation of action potentials. This principle of neuron activity is replicated in MNCS. **Dysfunctional $\mathbf{Ca^{2+}}$ channel:** The previous section has provided a detailed explanation of this trait. It is primarily caused by the dysregulation of Ca^{2+} channels, leading to their over or partial activation. This leads to a significant influx of Ca^{2+} into the neurons, maintaining a high level of depolarization and resulting in the abnormal firing of nerve cells. In MNCS, simulating the run-away behavior of the Ca^{2+} channel and achieving abnormal firing can be achieved by setting the R_{off} value of the Ca^{2+} channel memristor to a value close to R_{on}. **Mixed mode:** For this characteristic, the biological mechanism involves the K^+ channel group being in an intermediate state between abnormal and normal functioning. As mentioned earlier, if the Ca^{2+}-gated K^+ channels are blocked, the neuron will exhibit bursting behavior. Therefore, by adjusting the threshold value and activation speed of the K^+ channel memristor to an appropriate range, we can position it between controlled and out-of-control states. This enables us to effectively replicate this characteristic using the CN circuit. However, in the PN circuit, during the initial stage of firing, the action potential can be generated at a high frequency due to the rapid charging of the input capacitor C_{in}. Once the input capacitor C_{in} is fully charged, it will subsequently fire spiking in a normal manner. This design approach lacks biological support and exhibits poor performance in-circuit testing.

Bistability: Most neurons inherently exhibit the firing characteristics of bistability, which require the involvement of a non-voltage-gated K^+ channel. In a resting state, the activation of non-voltage-gated K^+ channels facilitates the outward flow of K^+ from neurons, leading to the establishment of a resting potential of approximately -71mV. When a neuron is stimulated by a non-voltage signal, the non-voltage-gated K^+ channel becomes either inactivated or semi-inactivated, resulting in a continuous rise in membrane potential until it reaches the threshold for firing an action potential. Therefore, according to biological theory, it is not possible to achieve bistability characteristics in MNCS using voltage-gated memristors. In MNCS, we still utilize voltage-gated memristors to simulate the physiological function of this specific K^+ channel. The triggering mechanism of this firing characteristic in MNCS deviates from biological principles.

Excitation block: From a biological perspective, in order for neurons to experience an excitation block, the ion channels need to undergo inactivation or partial inactivation. This process hinders the exchange of ions between the inside and outside of the neuron cell. However, the membrane potential of cells is determined by the distribution of ions inside and outside the cells prior to the inactivation of ion channels. If there is a high concentration of cations inside the cells, the membrane potential will be high; otherwise, it will be low. In the experiment, this characteristic can be achieved by blocking the variation of the resistance value of the memristor. Another possibility is that there are abnormalities in the ion channels, causing a constant exchange of cations and anions between the inside and outside of the neurons, resulting in a dynamic balance similar to the formation of resting potentials in neurons. Under this condition, the steady-state value of the membrane potential is determined by the magnitude of the anion and cation currents. Compared to the former possibility, the implementation of this mechanism is relatively complex. Therefore, in MNCS, the former speculation is utilized to implement the excitation block.

B. The practical experiment of the Memristor-based Neural Circuit System.

In the simulation, we systematically describe the various characteristic firing mechanisms of neurons and MNCS. To conduct the circuit experiment, we constructed a memristor circuit simulator using CMOS, bidirectional silicon-controlled rectifier, and other components to emulate the behavior of each ion channel memristor in the circuit. The structure of the ion channel memristor circuit simulator is depicted in Fig. 6. Fig. 6a illustrates the experimental scene, output results, and PCB circuit board used in our experiment. Fig. 6b, 6c, and 6d represent the simulators for the memristors corresponding to Na^+, Ca^{2+}, and K^+ channels, respectively. As shown in Fig. 6, the green area represents the activation control circuit, indicating that the corresponding memristor is switched to R_{on}. On the other hand, the orange area indicates the inactivation control circuit, causing the corresponding memristor to switch back to R_{off}. The circuit simulator is designed based on the fundamental characteristics of the bidirectional thyristor, incorporating the ideas provided by HP Labs [51]. As long as a certain level of current flows through the bidirectional thyristor, even when the control terminal voltage is removed, the bidirectional thyristor can remain in the conducting state. This characteristic can effectively simulate the memristance of ion channels. Therefore, it is only necessary to design a threshold circuit to control the bidirectional thyristor in order to effectively simulate ion channels. The complete experimental circuit diagram requires replacing the memristor in Fig. 4 with the memristor simulation circuit provided in Fig. 6. Table III presents the relevant parameters associated with MNCS in the practical experiment. The relevant parameters of circuit simulator for ion channel memristors are listed in Table IV.

The structure of the circuit experiment is illustrated in Fig. 7. We have already provided a comprehensive description of the various characteristics and corresponding operating mechanisms of neuronal cells and MNCS in the simulation experiment. We will not go into more specifics on these. The MNCS, modeled after the structure of neuronal cells and the HH model, proves to accurately imitate the biological traits of neurons. Among the circuits, the CN circuit is noteworthy as it emulates the structure and dynamic actions of neurons, and can imitate up to 24 distinct types of neuronal activities

C. Biological Characteristics Testing

For isolated neurons, they exhibit highly reliable and repeatable responses to fluctuating input currents, as do neurons in neural networks under strong stimuli. However, in the entire biological neural network, there is constant background firing and electrical leakage, which are generally considered noise signals for individual neurons. When neurons are subjected to stimuli lacking any temporal structure, they generate irregular spike signal sequences and exhibit irregular spontaneous activities that are not significantly correlated with external stimuli. To further verify whether MNCS possesses the characteristics of the aforementioned biological neurons, we conduct a Joint Interspike Interval (JISI) test [52]. The specific method is to replace stimuli without any temporal structure in the neural network with noise models. The specific approach involves introducing the noise signal as a background signal into the input signal of the MNCS, and then comparing it with the response of the biological neuron.

We constructed the simulated circuit according to the circuit shown in Fig. 4b. The specific parameter settings are adopted according to the configuration corresponding to tonic spiking in Table II. A current of 3μA in intensity is used as the baseline current input to the MNCS, stimulating it to produce continuous action potentials. To better observe the correlation between noise signals and consecutive spike intervals (ISIs), we applied three different gradients of noise signals ranging from 0 to 1μA as inputs to MNCS. Since the MNCS responses were largely similar under the same input conditions, we only captured the first 500ms of the output as the experimental results for presentation. The experimental results are depicted in Fig. 8. From the pulse graph on the left side of Fig. 8a, it can be observed that when a constant input without noise is applied to MNCS, it consistently generates consecutive spikes

TABLE III
THE PARAMETERS OF MEMRISTOR-BASED NEURON CIRCUIT SYSTEM PRACTICAL TEST.

Category	R_{in}	C_{in}	C_1	C_2	C_3	R_M	V_1^a	V_2^b	V_3^c	V_4^d	Circuit
Phasic spiking	$6k\Omega$	$1.5\mu F$	$1.5\mu F$	$1.5\mu F$	$1.5\mu F$	$2.7k\Omega$	$-7.1V$	$5.5V$	$-7.7V$	-	PN
	-	-	$2\mu F$	$2\mu F$	$2\mu F$	$2.7k\Omega$	$-7.1V$	$5.5V$	$-7.7V$	-	CN
Phasic bursting	$2.7k\Omega$	$5.5V$	$1.5\mu F$	$1.5\mu F$	$1.5\mu F$	$2.7k\Omega$	$-7.1V$	$5.5V$	$-7.7V$	-	PN
	-	-	$1.5\mu F$	$1.5\mu F$	$1.5\mu F$	$2.7k\Omega$	$-7.1V$	$5.5V$	$-7.7V$	$-7.7V$	CN
Spike frequency adaptation	$15k\Omega$	$5\mu F$	$1.5\mu F$	$1.5\mu F$	$1.5\mu F$	$2.7k\Omega$	$-7.1V$	$5.5V$	$-7.7V$	-	PN
Depolarizing after-potential	$10k\Omega$	$1.5\mu F$	$1.5\mu F$	$1.5\mu F$	$1.5\mu F$	$2.7k\Omega$	$-7.1V$	$5.5V$	$-7.7V$	-	PN
Accommodation	$20k\Omega$	$0.1\mu F$	$1.5\mu F$	$1.5\mu F$	$1.5\mu F$	$2.7k\Omega$	$-7.1V$	$5.5V$	$-7.7V$	-	PN
Tonic spiking	-	-	$1.5\mu F$	$1.5\mu F$	$1.5\mu F$	$2.7k\Omega$	$-7.1V$	$5.5V$	$-7.7V$	-	CN
Tonic bursting	-	-	$1.5\mu F$	$1.5\mu F$	$1.5\mu F$	$2.7k\Omega$	$-7.1V$	$5.5V$	$-7.7V$	-	CN
Rebound spike	-	-	$1.5\mu F$	$1.5\mu F$	$1.5\mu F$	$2.7k\Omega$	$-7.1V$	$5.5V$	$-7.7V$	$11.8V$	CN
Rebound bursting	-	-	$1.5\mu F$	$1.5\mu F$	$1.5\mu F$	$2.7k\Omega$	$-7.1V$	$5.5V$	$-7.7V$	$11.8V$	CN
Class 1 excitable	-	-	$2\mu F$	$2\mu F$	$2\mu F$	$2.7k\Omega$	$-7.1V$	$5.5V$	$-7.7V$	-	CN
Class 2 excitable	-	-	$0.5\mu F$	$0.5\mu F$	$0.5\mu F$	$2.7k\Omega$	$-7.1V$	$5.5V$	$-7.7V$	-	CN
Spike latency	-	-	$1.5\mu F$	$1.5\mu F$	$1.5\mu F$	$2.7k\Omega$	$-7.1V$	$5.5V$	$-7.7V$	$11.8V$	CN
Refractory period	-	-	$1.5\mu F$	$1.5\mu F$	$1.5\mu F$	$2.7k\Omega$	$-7.1V$	$5.5V$	$-7.7V$	-	CN
All-or-nothing firing	-	-	$1.5\mu F$	$1.5\mu F$	$1.5\mu F$	$2.7k\Omega$	$-7.1V$	$5.5V$	$-7.7V$	-	CN
Inhibition-induced spiking	-	-	$1.5\mu F$	$1.5\mu F$	$1.5\mu F$	$2.7k\Omega$	$-7.1V$	$5.5V$	$-7.7V$	$11.8V$	CN
Inhibition-induced bursting	-	-	$1.5\mu F$	$1.5\mu F$	$1.5\mu F$	$2.7k\Omega$	$-7.1V$	$5.5V$	$-7.7V$	$11.8V$	CN
Resonator	-	-	$1.5\mu F$	$1.5\mu F$	$1.5\mu F$	$2.7k\Omega$	$-7.1V$	$5.5V$	$-7.7V$	-	CN
Integrator	-	-	$1.5\mu F$	$1.5\mu F$	$1.5\mu F$	$2.7k\Omega$	$-7.1V$	$5.5V$	$-7.7V$	-	CN
Threshold variability	-	-	$1.5\mu F$	$1.5\mu F$	$1.5\mu F$	$2.7k\Omega$	$-7.1V$	$5.5V$	$-7.7V$	$11.8V$	CN
Subthreshold oscillations	-	-	$1.5\mu F$	$1.5\mu F$	$1.5\mu F$	$2.7k\Omega$	$-7.1V$	$5.5V$	$-7.7V$	$11.8V$	CN
Dysfunctional Ca channel	-	-	$1.5\mu F$	$1.5\mu F$	$1.5\mu F$	$2.7k\Omega$	$-7.1V$	$5.5V$	$-7.7V$	$11.8V$	CN
Mixed mode	$23k\Omega$	$5\mu F$	$1.5\mu F$	$1.5\mu F$	$1.5\mu F$	$2.7k\Omega$	$-7.1V$	$5.5V$	$-7.7V$	-	PN
	-	-	$1.5\mu F$	$1.5\mu F$	$1.5\mu F$	$2.7k\Omega$	$-7.1V$	$5.5V$	$-7.7V$	$-7.7V$	CN
Bistability	-	-	$1.5\mu F$	$1.5\mu F$	$1.5\mu F$	$2.7k\Omega$	$-7.1V$	$5.5V$	$-7.7V$	$-7.7V$	CN
Excitation block	-	-	$1.5\mu F$	$1.5\mu F$	$1.5\mu F$	$2.7k\Omega$	$-7.1V$	$5.5V$	$-7.7V$	$-7.7V$	CN

Note : The symbol '-' represents an empty value.

TABLE IV
THE PARAMETERS OF CIRCUIT SIMULATOR FOR ION CHANNEL MEMRISTORS.

Category	R_1	R_2	R_3	R_4	R_5	R_6	R_7	R_8	DC_1	DC_2	DC_3	DC_4	DC_5
Na^+ CH circuit	$2M\Omega$	$0.1M\Omega$	$1M\Omega$	$0.2k\Omega$	$10k\Omega$	$1k\Omega$	$1.11M\Omega$	$0.39M\Omega$	$6.3V$	$4V$	$5.5V$	$10V$	-
K^+ CH circuit	5Ω	$2M\Omega$	-	-	-	-	-	-	$7.7V$	$2.5V$	$9V$	-	-
Ca^{2+} CH circuit	$10k\Omega$	10Ω	100Ω	10Ω	$2M\Omega$	50Ω	-	-	$11.8V$	$15V$	$13V$	$15V$	$5V$

Note 1: The symbol '-' represents an empty value.
Note 2: The KT stands for electromagnetic relay.

with approximately equal time intervals. This characteristic is further illustrated by the JISI scatter plot on the right side of Fig. 8a. This characteristic aligns with the phenomenon observed in isolated individual biological neuron experiments. When a noise signal of $0.5\mu A$ is added to a constant input, the consecutive spike intervals generated by MNCS exhibit irregularities. From the pulse plot and scatter plot in Fig. 8b, it is evident that certain consecutive spike intervals exhibit varying degrees of elongation. When the noise signal intensity increases to 1uA, the anomalous consecutive spike intervals continuously generated by MNCS become more prominent. The scatter plot in Fig. 8c closely resembles the irregular spike signal sequence generated by biological neurons [52].

The experimental results of JISI have effectively demonstrated that under the influence of noise signals, MNCS generates irregular spike signal sequences and irregular spontaneous activities. These responses do not exhibit a significant correlation with external stimuli.

IV. COMPARISON WITH PREVIOUS WORK

In Table V, various neuron mathematical and circuit models are analyzed and compared. It is obvious that early established models such as Integrate and Fire, and Quadratic Integrate and Fire, fail to capture many essential biological characteristics due to their limited representation of cellular dynamics. However, with the continuous progress of theoretical and experimental techniques, researchers have developed mathematical models that can accurately represent almost all biological characteristics. Notable examples of such models are the Izhikevich (2003) and Hodgkin-Huxley models.

In recent years, there has been a growing trend of utilizing circuitry to implement classic neural dynamics mathematical models, thanks to advancements in material technology. An example is the Izhikevich (2022) circuit presented in Table V, which is implemented using FPGA technology, capable of reproducing 8 highly complex neuronal firing behaviors [53], has the potential to replicate all the neuronal characteristics outlined in the Izhikevich (2003) mathematical model. Unfortunately, despite the significant energy-saving advantages of the Izhikevich circuit, its implementation principle is based on logical circuits, which means that the Izhikevich (2022) circuit lacks biologically meaningful interpretability [53]. As indicated in Table V, the HRL VO_2 Neuron incorporates the structural elements and dynamics of the HH model, allowing it to replicate common neuronal biological characteristics. HRL VO_2 Neuron is composed of three circuit systems. Among these, the Tonic Neuron circuit system can exhibit up to 15 distinct discharge characteristics. However, due to the HRL VO_2 Neuron has limitations in terms of referencing biological structure and dynamic principles, the individual neuron circuit systems within the HRL VO_2 Neuron exhibit a relatively small number of neuronal firing characteristics. This paper fully

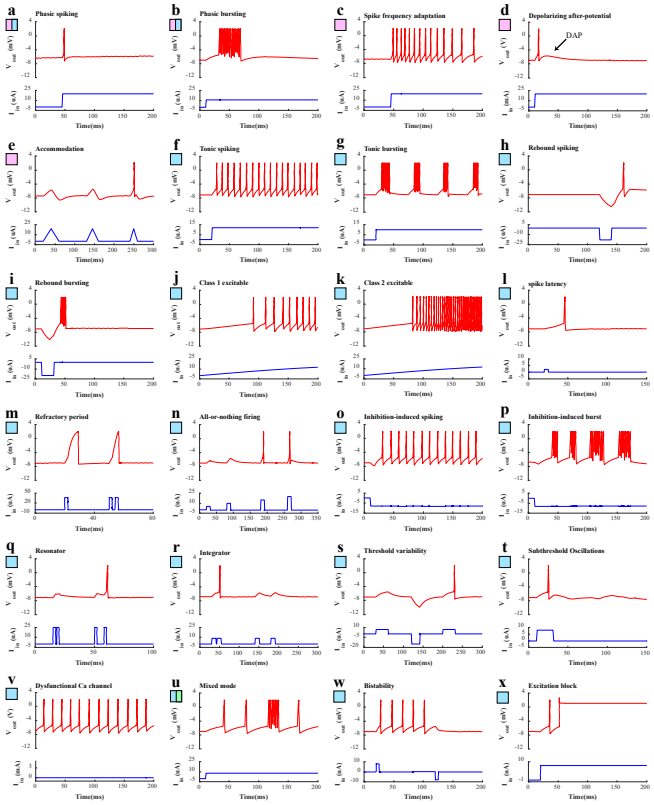

Fig. 5. Simulation Test Results For 22 Neuronal Firing Behaviors.a) Phasic spiking; b) Phasic bursting; c) Spike frequency adaptation; d) Depolarizing after-potential; e) Accommodation; f) Tonic spiking; g) Tonic bursting; h) Rebound spike; i) Rebound bursting; j) Class 1 excitable; k) Class 2 excitable; l) Spike latency; m) Refractory period; n) All-or-nothing firing; o) Inhibition-induced spiking; p) Inhibition-induced bursting; q) Resonator; r) Integrator; s) Threshold variability; t) Subthreshold oscillations; u) Dysfunctional Ca channel; v) Mixed mode 1; w) Mixed mode 2.

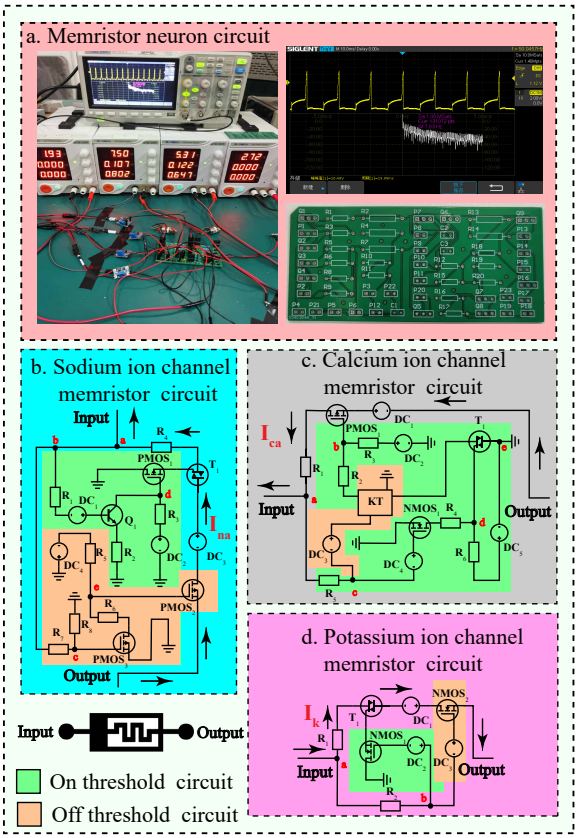

Fig. 6. Circuit testing and memristor circuit simulators. a) MNCS circuit testing scenarios, output results, and PCB boards; b) Structure diagram of Na^+ channel memristor circuit simulato; c) Structure diagram of Ca^{2+} channel memristor circuit simulator; d) Structure diagram of K^+ channel memristor circuit simulator.

adheres to the structure and dynamics of biological neurons in

TABLE V
COMPARISON WITH THE BIOLOGICAL CHARACTERISTICS OF CLASSICAL NEURON MODELS OR CIRCUITS [19].

	All-or-nothing firing	Refractory	Excitation	Biophysically meaningful	Tonic spiking	Phasic spiking	Tonic bursting	Phasic bursting	Mixed mode	Spike frequency adaptation	Class 1 excitable	Class 2 excitable	Spike latency	Subthreshold oscillations	Resonator	Integrator	Rebound spike	Rebound burst	Threshold variability	Bistability	DAP	Accommodation	Inhibition-induced spiking	Inhibition-induced bursting	Chaos	Dysfunctional Ca_{2+}channel	# of FLOPS
Integrate-and-fire	+	+	-	-	+	-	-	-	-	-	+	-	-	-	-	+	-	-	-	-	-	-	-	-	-	*	5
Integrate-and-fire with adapt	+	+	-	-	+	-	-	-	-	+	+	-	-	-	-	+	-	-	-	-	+	-	-	-	-	*	10
Integrate-and-fire-or-burst	+	+	-	-	+	+	*	+	-	+	+	-	-	-	-	+	+	+	-	+	+	-	-	-	-	*	13
Resonate-and-fire	+	+	+	-	+	+	-	-	-	-	+	+	-	+	+	+	+	-	-	+	+	+	-	-	+	*	10
Quadratic integrate-and-fire	+	+	-	-	+	-	-	-	-	-	+	-	+	-	-	+	-	-	+	+	-	-	-	-	-	*	7
Izhikevich(2003)	+	+	+	-	+	+	+	+	+	+	+	+	+	+	+	+	+	+	+	+	+	+	+	+	+	*	13
FitzHugh-Nagumo	+	+	+	-	+	+	-	*	-	-	+	-	+	+	+	-	+	-	+	+	-	+	+	-	-	*	72
Hindmarsh-Rose	+	+	+	-	+	+	+	*	*	+	+	+	+	+	+	+	+	+	+	+	+	+	+	*	+	*	120
Morris-Lecar	+	+	+	+	+	+	-	*	-	-	+	+	+	+	+	+	+	*	+	+	-	+	+	-	-	*	600
Wilson	+	+	+	-	+	+	+	*	*	+	+	+	+	+	+	+	+	+	+	*	+	+	*	*	*	*	180
Hodgkin-Huxley	+	+	+	+	+	+	+	*	*	+	+	+	+	+	+	+	+	+	+	+	+	+	+	*	+	*	1200
Izhikevich(2022)	*	*	*	-	+	+	+	*	*	*	*	*	*	+	*	*	*	*	*	*	+	*	*	+	*	*	
—TN	+	+	+	+	+	-	+	-	-	+	+	+	+	+	-	+	-	-	-	+	-	-	+	+	*	*	
HRL VO_2 Neuron —PN	-	-	-	-	-	+	-	+	-	-	-	-	-	-	+	-	+	+	+	-	+	+	-	-	*	*	
—MN	-	-	-	-	-	-	-	-	+	-	-	-	-	-	-	-	-	-	-	-	-	-	-	-	*	*	
—CN	+	+	+	+	+	+	+	+	+	-	+	+	+	+	+	+	+	+	+	+	-	-	+	+	*	+	
MNCS —PN	-	-	-	-	-	+	-	+	-	+	-	-	-	-	-	-	-	-	-	-	+	+	-	-	*	*	
—MN	-	-	-	-	-	-	-	-	+	-	-	-	-	-	-	-	-	-	-	-	-	-	-	-	*	*	

Note 1 : The symbols ”+”, ”-”, and ”*” represent ”has,” ”does not have,” and ”uncertain if it has,” respectively.

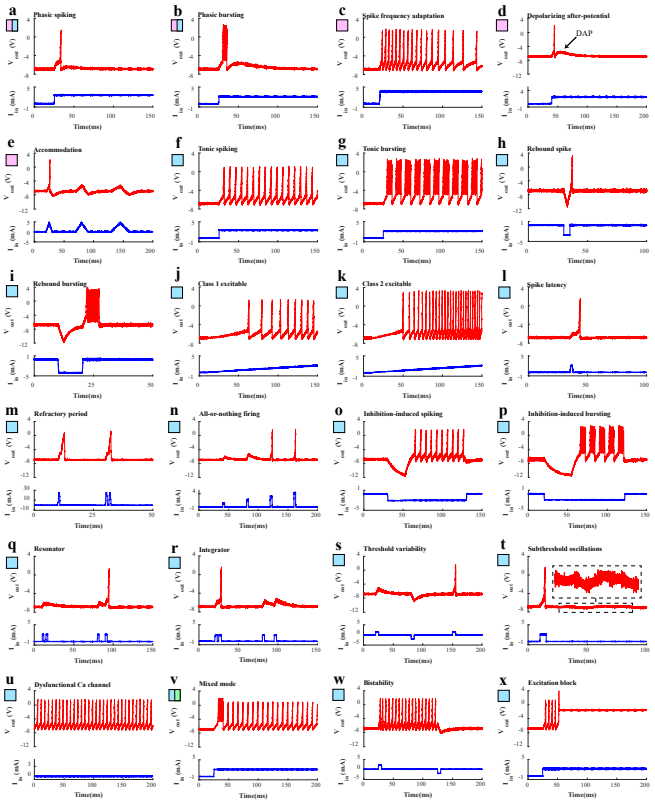

Fig. 7. Circuit Experiment Results For 22 Neuronal Firing Behaviors. a) Phasic spiking; b) Phasic bursting; c) Spike frequency adaptation; d) Depolarizing after-potential; e) Accommodation; f) Tonic spiking; g) Tonic bursting; h) Rebound spike; i) Rebound bursting; j) Class 1 excitable; k) Class 2 excitable; l) Spike latency; m) Refractory period; n) All-or-nothing firing; o) Inhibition-induced spiking; p) Inhibition-induced bursting; q) Resonator; r) Integrator; s) Threshold variability; t) Subthreshold oscillations; u) Dysfunctional Ca channel; v) Mixed mode 1; w) Mixed mode 2.

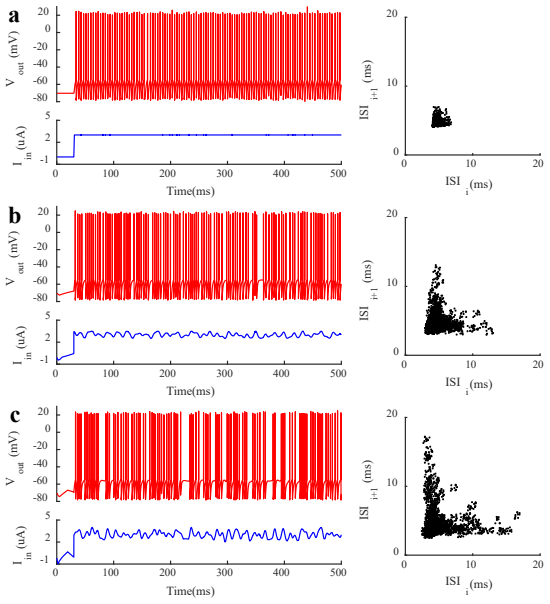

Fig. 8. The correlation between noise signals and consecutive spike intervals (ISIs). a) without noise signal; b) a $0.5\mu A$ noise signal; c) $1\mu A$noise signal

designing MNCS, through PSpice simulation and practical experiments, it has been demonstrated that MNCS can replicate almost all common neuronal biological characteristics.

V. CONCLUSION

In this paper, we propose a memristor-based neuron circuit system to address the hard problem of energy efficiency calculation beyond the capabilities of von Neumann architecture. By utilizing the intricate biological structure and intricate micro dynamics of neurons, a complex memristor neuron circuit system is constructed based on the cellular structure of neurons. We begin with an in-depth examination of the biological traits of ion channels that play a role in generating action potentials. Next, we make use of the unique nonlinear and non-volatile properties of memristors to accurately replicate the biological functions of these ion channels. We also incorporate capacitors to imitate the ion isolation function found in lipid bilayers and a DC voltage source to mimic the Nernst potential which arises from the difference in ion concentration between the interior and exterior of nerve cells. Finally, we take these circuit components and create a complex memristor neuron circuit system that is modeled after the cellular structure of neurons. Through PSpice simulation, circuit experiments, and JISI experiments, it has been demonstrated that MNCS can accurately replicate almost all of the common biological characteristics that are displayed by neurons. MNCS exhibits continuous discharge characteristics similar to biological neurons under the influence of continuously increasing background noise. The proposed MNCS can act as the building block for the neural circuits found in spiking neural networks (SNN), providing more biological features to the SNN, resulting in more intricate discharge modes and the potential for chaotic firing.

REFERENCES

[1] Y. Zheng, H. Ravichandran, and T. Schranghamer et al., "Hardware implementation of bayesian network based on two-dimensional memtransistors," in *Nat Commun*, vol. 13, 2022, p. 5578.
[2] S. Kumar, X. Wang, and J. Strachan et al., "Dynamical memristors for higher-complexity neuromorphic computing," in *Nat Rev Mater*, vol. 7, 2022, pp. 575–591.
[3] Y. Fangwen et al., "Brain-inspired multimodal hybrid neural network for robot place recognition," in *Sci. Robot*, vol. 8, 2023, p. eabm6996.
[4] T. Mei and C. Chen, "In-memory mechanical computing," in *Nat Commun*, vol. 14, 2023, p. 5204.
[5] H. Lee, J. Kim, H. Kim, and K. Kim et al., "Nanograin network memory with reconfigurable percolation paths for synaptic interactions," in *Light Sci Appl*, 2023, p. 12(1):118.
[6] S. Cho, C. Jo, and Y. Kim et al., "Progress of materials and devices for neuromorphic vision sensors," in *Nano-Micro Lett*, vol. 14, 2022, p. 203.
[7] F. Zhu, H. Grier, and R. Tandon et al., "A deep learning framework for inference of single-trial neural population dynamics from calcium imaging with subframe temporal resolution," in *Nat Neurosci*, vol. 25, 2022, p. 1724–1734.
[8] M. Payvand, F. Moro, and K. Nomura et al., "Self-organization of an inhomogeneous memristive hardware for sequence learning," in *Nat Commun*, vol. 13, 2022, p. 5793.
[9] M. Saponati and M. Vinck, "Sequence anticipation and spike-timing-dependent plasticity emerge from a predictive learning rule," in *Nat Commun*, vol. 14, 2023, p. 4985.
[10] M. Pagkalos, S. Chavlis, and P. Poirazi, "Introducing the dendrify framework for incorporating dendrites to spiking neural networks," in *Nat Commun*, vol. 14, 2023, p. 131.

[11] P. Diehl, D. Neil, and J. Binas et al., "Fast-classifying, high-accuracy spiking deep networks through weight and threshold balancing," in *International Joint Conference on Neural Networks. IEEE, year = 2015,*.
[12] G. Syed, Y. Zhou, and J. Warner et al., in *Atomically thin optomemristive feedback neurons*, 2023.
[13] A. Gidon, T. Zolnik, and P. Fidzinski et al., "Dendritic action potentials and computation in human layer 2/3 cortical neurons," in *Science*, vol. 367(6473), 2020, pp. 83–87.
[14] D. Wang, R. Tang, and H. Lin et al., "Spintronic leaky-integrate-fire spiking neurons with self-reset and winner-takes-all for neuromorphic computing," in *Nat Commun*, vol. 14, 2023, p. 1068.
[15] M. Wei, W. Verstraelen, and K. Orfanakis et al., "Optically trapped room temperature polariton condensate in an organic semiconductor," in *Nat Commun*, vol. 13, 2022, p. 7191.
[16] Q. Hong, H. Chen, and J. Sun et al., "Memristive circuit implementation of a self-repairing network based on biological astrocytes in robot application," in *IEEE Transactions on Neural Networks and Learning Systems*, vol. 99, 2020, pp. 1–15.
[17] L. Chua, "If it's pinched it's a memristor," in *Springer New York*, 2014.
[18] S. Sung, T. Kim, and H. Shin et al., "Simultaneous emulation of synaptic and intrinsic plasticity using a memristive synapse," in *Nat Commun*, vol. 13, 2022, p. 2811.
[19] W. Yi, K. Tsang, and S. Lam et al., "Biological plausibility and stochasticity in scalable vo2 active memristor neurons," in *Nature Communications*, vol. 9, 2018, p. 1.
[20] X. Li, Y. Zhong, and H. Chen et al., "A memristors-based dendritic neuron for high-efficiency spatial-temporal information processing," in *Adv. Mater.*, 2022, p. 2203684.
[21] Y. Wang, Q. Zhang, and H. Astier et al., "Dynamic molecular switches with hysteretic negative differential conductance emulating synaptic behaviour," in *Nat. Mater.*, vol. 21, 2022, p. 1403–1411.
[22] S. Seo, B. Kim, and D. Kim et al., "The gate injection-based field-effect synapse transistor with linear conductance update for online training," in *Nat Commun*, vol. 13, 2022, p. 6431.
[23] R. Lin, H and C. Wang et al., "Hyperchaotic memristive ring neural network and application in medical image encryption," in *Nonlinear Dynamics*, vol. 110(1), 2022, pp. 841–855.
[24] ——, "Neural bursting and synchronization emulated by neural networks and circuits," in *IEEE Transactions on Circuits and Systems I-Regular Papers*, vol. 68(8), 2021, pp. 3397–3410.
[25] Q. Xia et al., "Memristor-cmos hybrid integrated circuits for reconfigurable logic," in *Nano. Lett.*, vol. 9, 2009, p. 3640–3645.
[26] A. Khiat, P. Ayliffe, and T. Prodromakis, "High density crossbar arrays with sub-15 nm single cells via liftoff process only," in *Sci. Rep*, vol. 6, 2016, p. 32614.
[27] J. Ying, Y. Liang, and G. Wang et al., "Action potential and chaos near the edge of chaos in memristive circuits," in *Chaos 1 September*, vol. 32(9), 2022, p. 093101.
[28] J. Zhao, Y. Ran, Y. Pei, Y. Wei, J. Sun, Z. Zhang, J. Wang, Z. Zhou, Z. Wang, Y. Sun, and X. Yan, "Memristors based on ndnio3 nanocrystals film as sensory neurons for neuromorphic computing," in *Mater Horiz*, 2023 Aug 9.
[29] Y. Liang, Z. Chen, and G. Wang et al., "A new compact model for third-order memristive neuron with box-shaped hysteresis and dynamics analysis," in *IEEE Transactions on Computer-Aided Design of Integrated Circuits and Systems*, 2023, p. 3245543.
[30] M. Pickett, G. Medeiros-Ribeiro, and R. Williams, "A scalable neuristor built with mott memristors," in *Nature Mater*, vol. 12, 2013, p. 114–117.
[31] H. Lim et al., "Reliability of neuronal information conveyed by unreliable neuristor-based leaky integrate-and-fire neurons: a model study," in *Sci. Rep.*, vol. 5, 2015, p. 09776.
[32] L. Badel and T. Lefort, S.and Berger et al., "Extracting non-linear integrate-and-fire models from experimental data using dynamic i–v curves," in *Biological Cybernetics*, vol. 5, 2015, p. 09776.
[33] L. O. Chua, V. Sbitnev, and H. Kim, "Hodgkin–huxley axon is made of memristors," in *Int. J. Bifur. Chaos*, vol. 22, 2012, p. 1230011.
[34] P. Protachevicz, C. Bonin, and K. Iarosz et al., "Large coefficient of variation of inter-spike intervals induced by noise current in the resonate-and-fire model neuron," in *Cogn Neurodyn*, vol. 16, 2022, p. 1461–1470.
[35] E. M. Izhikevich, "Which model to use for cortical spiking neurons?" in *IEEE.Trans. Neural Netw.*, vol. 15, 2004, p. 1063–1070.
[36] B. W. Connors and M. J. Gutnick, "Intrinsic firing patterns of diverse cortical neurons," in *Trends Neurosci*, vol. 13, 1990, p. 99–104.
[37] B. Bao, J. Hu, and J. Cai et al., "Memristor-induced mode transitions and extreme multistability in a map-based neuron model," in *Nonlinear Dynamics*, vol. 111(4), 2023, pp. 3765–3779.
[38] K. LI, B. Bao, and J. Ma et al., "Synchronization transitions in a discrete memristor-coupled bi-neuron model," in *Chaos, Solitons and Fractals*, vol. 165, 2022, p. 112861.
[39] W. Gerstner, W. Kistler, and R. Naud et al., "Neuronal dynamics: From single neurons to networks and models of cognition," 2014.
[40] B. Hille, "Modification of gating in voltage-sensitive channels. ionic channels of excitable membranes," 2001.
[41] C. Aizenman and D. Linden et al., "Regulation of the rebound depolarization and spontaneous firing patterns of deep nuclear neurons in slices of rat cerebellum," in *Neurophysiol*, vol. 82, 1999, p. 1697–1709.
[42] K. Talavera and B. Nilius, "Biophysics and structure-function relationship of t-type ca2+ channels," in *Cell Calcium*, vol. 40(2), 2006, pp. 97–114.
[43] B. Kampa, G. W, and F. Helmchen, "Three-dimensional imaging of neuronal network activity. in: Imaging in neuroscience: A laboratory manual," 2011.
[44] A. Destexhe, D. Contreras, and T. J. Sejnowski et al., "A model of spindle rhythmicity in the isolated thalamic reticular nucleus," in *Neurophysiol*, vol. 72(2), 1994a, p. 803–818.
[45] A. Blatz and K. Magleby, "Single apamin-blocked ca-activated k—[plus]— channels of small conductance in cultured rat skeletal muscle," in *Nature*, vol. 323(6090), 1986, pp. 718–720.
[46] L. Cai, L. Yu, and Y. Yang et al., "Integrated memristor network for physiological signal processing," in *Advanced Electronic Materials*, 2023, p. 2300021.
[47] Q. Hong, Z. Shi, and J. Sun et al., "Memristive self-learning logic circuit with application to encoder and decoder," in *Neural Computing and Applications*, vol. 12, 2022.
[48] P. Schwartzkroin and A. Wyler, "Mechanisms underlying epileptiform burst discharge," in *Annals of Neurology*, vol. 7(2), 2010, pp. 95–107.
[49] M. Yazawa, B. Hsueh, and X. Jia et al., "Using induced pluripotent stem cells to investigate cardiac phenotypes in timothy syndrome," in *Nature*, vol. 471(7337), 2011, pp. 230–234.
[50] I. Dzhura, Y. Wu, and R. Colbran et al., "Calmodulin kinase determines calcium-dependent facilitation of l-type calcium channels," in *Nat Cell Biol*, vol. 2, 2000, p. 173–177.
[51] M. Fitzurka and D. Tam, "Memristor emulators: a note on modeling," in *in Advances in Memristors, Memristive Devices and Systems*, 2017.
[52] A. Ascoli, R. Tetzla, and L. Chua et al., "A joint interspike interval difference stochastic spike train analysis: detecting local trends in the temporal firing patterns of single neurons," in *Biological Cybernetics*, vol. 80(5), 1999, pp. 309–326.
[53] J. Wang and et al., "A high-accuracy and energy-efficient cordic based izhikevich neuron with error suppression and compensation," in *IEEE Transactions on Biomedical Circuits and Systems*, vol. 5, 2022, pp. 807–821.

Xiaosong Li received the B.S. degree from Mechanical Design, Manufacturing, and Automation, Jimei University(JMU), Xiamen, China, in 2017 and the M.S degree from Mechanical Manufacturing, and Automation, Southwest Forestry University, Kunming, China, in 2021. Currently, he is working toward the Eng.D. degree in Energy and Power at College of Computer Science and Electronic Engineering, Hunan University, Changsha 410082, China and Chongqing Research Institute, Hunan University, Chongqing 401120, China. His research interests include cognitive neuroscience, memristive logic circuits, and neuromorphic networks.

Jingru Sun graduated from Hunan University, China. in 2014 with a Ph.D. degree in computer science and technology. She is an associate professor in College of Computer Science and Electronic Engineering, Hunan University, Changsha, 410082 and Chongqing Research Institute, Hunan University, Chongqing 401120, China. She has published more than 30 papers and her research interests include memristive neural networks, brain-like computing, and intelligent transportation.

Yichuang Sun received the B.Sc. and M.Sc. degrees from Dalian Maritime University, Dalian, China, in 1982 and 1985, respectively, and the Ph.D. degree from the University of York, York, U.K., in 1996, all in communications and electronics engineering.

He is currently a Professor of communications and electronics, the Head of the Communications and Intelligent Systems Research Group, and Head of the Electronic, Communication and Electrical Engineering Division, School of Engineering and Computer Science, University of Hertfordshire, U.K. He has published over 350 articles and contributed ten chapters in edited books. He has also published four text and research books: Continuous-Time Active Filter Design (CRC Press, USA, 1999), Design of High Frequency Integrated Analogue Filters (IEE Press, U.K., 2002), Wireless Communication Circuits and Systems (IET Press, 2004), and Test and Diagnosis of Analogue, Mixed-signal, and RF Integrated Circuits: The Systems on Chip Approach (IET Press,2008). His research interests include wireless and mobile communications, RF and analog circuits, microelectronic devices and systems, machine learning, and deep learning.

Dr. Sun was a Series Editor of IEE Circuits, Devices and Systems Book Series from 2003 to 2008. He had been Associate Editor of IEEE Transactions on Circuits and Systems I: Regular Papers from 2010 to 2011, from 2016 to 2017, and from 2018 to 2019. He is also Editor of ETRI Journal, the Journal of Semiconductors, and the Journal of Sensor and Actuator Networks. He was a Guest Editor of eight IEEE and IEE/IET journal special issues: High-frequency Integrated Analogue Filters in IEE Proceedings on Circuits, Devices and Systems in 2000, RF Circuits and Systems for Wireless Communications in IEE Proceeding on Circuits, Devices and Systems in 2002, Analogue and Mixed-Signal Test for Systems on Chip in IEE Proceeding on Circuits, Devices and Systems in 2004, MIMO Wireless and Mobile Communications in IEE Proceeding on Communications in 2006, Advanced Signal Processing for Wireless and Mobile Communications in IET Signal Processing in 2009,Cooperative Wireless and Mobile Communications in IET Communications in 2013, Software-Defined Radio Transceivers and Circuits for 5G Wireless Communications in IEEE Transactions on Circuits and Systems-II: Express Briefs in 2016, and the 2016 IEEE International Symposium on Circuits and Systems in IEEE Transactions on Circuits and Systems-I: Regular Papers in 2016. He has also been widely involved in various IEEE technical committee and international conference activities.

Chunhua Wang received the M.S. degree from Zhengzhou University, Zhengzhou, China, in 1994, and the Ph.D. degree from Beijing University of Technology, Beijing, China, in 2003. He is currently a Professor of n 2019. He is currently an Associate Professor with College of computer science and electronic engineering Hunan University, Changsha, China. He is a Doctor tutor, Director of Advanced Communication Technology Key Laboratory of Hunan Universities, a member of Academic Committee of Hunan University, a Director of Chaos and Nonlinear Circuit Professional Committee of Circuit and System Branch of China Electronic Society. Now, his research interests include memristor circuit, complex networks, chaotic circuit, chaos secure communication, current-mode circuit and neural networks based on memristor. He has presided over 8 national and provincial projects, and published more than 120 papers, among which more than 100 were retrieved by SCI.

Qinghui Hong received the B.S degree and M.S degree in electronic science and technology from Xiangtan University, Xiangtan, China, in 2012 and 2015, respectively, and the Ph.D degree in computer system architecture from Huazhong University of Science and Technology, Wuhan, China, in 2019. He is currently an Associate Professor with College of computer science and electronic engineering, Hunan University, Changsha 410082, China. His current research interests include memristive neural network and its application to Artifificial Intelligence.

Sichun Du received the M.S and Ph.D degree in computer science and technology from Hunan University, Changsha, China, in 2005 and 2012, respectively. He is currently an Associate Professor with College of Computer Science and Electronic Engineering, Hunan University. His research interests include memristive neural network, analog/RF integrated circuit synthesis and evolutionary computation algorithms.

Jiliang Zhang received the Ph.D. degree in Computer Science and Technology from Hunan University, Changsha, China in 2015. From 2013 to 2014, he worked as a Research Scholar at the Maryland Embedded Systems and Hardware Security Lab, University of Maryland, College Park. From 2015 to 2017, he was an Associate Professor with Northeastern University, China. In April 2017, he joined the Hunan University. He is currently a Full Professor at the College of Integrated Circuits, Hunan University. He is Vice Dean of the College of Integrated Circuits at Hunan University, the Director of Chip Security Institute of Hunan University, and the Secretary-General of CCF Fault Tolerant Computing Professional Committee. His current research interests include Hardware Security, Integrated Circuit Design and Intelligent System. He has authored more than 60 technical papers in leading journals and conferences. He was the recipient of CCF Integrated Circuit Early Career Award and the winner of Excellent Youth Fund of the National Natural Science Foundation of China. He is serving as a steering member for Hardware Security Forum of China. He is a senior member of IEEE/CCF.